

Gravitational lensing by elliptical galaxies

Daniel J. Mortlock^{1,2,3*} and Rachel L. Webster^{1*}

¹*School of Physics, The University of Melbourne, Parkville, Victoria 3052, Australia*

²*Astrophysics Group, Cavendish Laboratory, Madingley Road, Cambridge CB3 0HE, U.K.*

³*Institute of Astronomy, Madingley Road, Cambridge CB3 0HA, U.K.*

Accepted. Received; in original form 2000 April 19

ABSTRACT

The fraction of high-redshift sources which are multiply-imaged by intervening galaxies is strongly dependent on the cosmological constant, and so can be a useful probe of the cosmological model. However its power is limited by various systematic (and random) uncertainties in the calculation of lensing probabilities, one of the most important of which is the dynamical normalisation of elliptical galaxies. Assuming ellipticals' mass distributions can be modelled as isothermal spheres, the mass normalisation depends on: the velocity anisotropy; the luminosity density; the core radius; and the area over which the velocity dispersion is measured. The differences in the lensing probability and optical depth produced by using the correct normalisation can be comparable to the differences between even the most extreme cosmological models. The existing data is not sufficient to determine the correct normalisation with enough certainty to allow lensing statistics to be used to their full potential. However, as the correct lensing probability is almost certainly higher than is usually assumed, upper bounds on the cosmological constant are not weakened by these possibilities.

Key words: gravitational lensing – galaxies: statistics – galaxies: kinematics and dynamics – galaxies: structure – cosmology: miscellaneous.

1 INTRODUCTION

The fraction of high-redshift quasars which are multiply-imaged due to gravitational lensing is determined mainly by the cosmological model and the population of potential lenses. Many of the early investigations into the statistics of quasar lensing (e.g. Press & Gunn 1973; Turner, Ostriker & Gott 1984; Kochanek & Blandford 1987; Fukugita & Turner 1991; Maoz & Rix 1993) focussed on the deflector population, but more recent studies have emphasised the cosmological possibilities. Specifically, Turner (1990) and Fukugita, Futumase & Kasai (1990) found that the lensing probability increases very rapidly with the (normalised) cosmological constant, Ω_{Λ_0} , but depends only weakly on the (normalised) matter density, Ω_{m_0} . One of the most stringent upper limits that can be placed on the value of the cosmological constant is due to the low number of lenses detected – both Kochanek (1996b) and Falco, Kochanek & Muñoz (1998) found that $\Omega_{\Lambda_0} \lesssim 0.65$, with 95 per cent confidence. These results are only marginally consistent with a number of independent cosmological measurements, such as high-redshift

supernova observations (e.g. Schmidt et al. 1998; Perlmutter et al. 1999) and cosmic microwave background measurements (e.g. Lineweaver 1998; Efstathiou et al. 1999), which imply that $\Omega_{\Lambda_0} = 0.7 \pm 0.2$, again at the 95 per cent confidence level. Further, the low density implied by cluster observations (e.g. Bahcall, Fan & Cen 1997), combined with the inflationary requirement of a flat universe (e.g. Guth 1981; Kolb & Turner 1989) also imply a high value of Ω_{Λ_0} . It is thus very important to accurately assess both the random and systematic uncertainties on the lensing constraints.

Some of the random uncertainties in the lens statistics are being steadily reduced as new surveys better constrain the deflector and source populations and more lenses are discovered. If ellipticals do completely dominate the lensing probability (e.g. Turner et al. 1984; Kochanek 1996b), any improvements in the knowledge of the number density of galaxies must be accompanied by accurate type information. Both the Sloan Digital Sky Survey (e.g. Szalay 1998; Loveday & Pier 1998) and the 2 degree Field galaxy redshift survey (e.g. Colless 1999; Folkes et al. 1999) should decrease the errors on the type-specific luminosity functions by up to an order of magnitude. These two projects will also greatly reduce the uncertainties in the quasar luminosity function, as well as yielding more lensed quasars than

* E-mail: mortlock@ast.cam.ac.uk (DJM); rwebster@physics.unimelb.edu.au (RLW)

are known to date (e.g. Loveday & Pier 1998; Boyle et al. 1999a,b; Mortlock & Webster 2000b).

However, comparable progress in reducing the various systematic uncertainties is unlikely to be as rapid or as certain. Firstly, dust in the lensing galaxies can obscure multiply-imaged quasars from lens surveys. There is some evidence that it is an unimportant effect (e.g. Kochanek et al. 1999; Falco et al. 1999), but it is also possible that it dominates the statistics (Malhotra, Rhoads & Turner 1997). There are a number of studies of dust in local galaxies, but it is reddening in high-redshift galaxies that is more important to lensing statistics. The only measurements of obscuration in such galaxies comes from lensed quasars, as the colours of the various images of the one source can be compared. Using this technique Falco et al. (1999) found that ellipticals with redshifts of up to ~ 1 have minimal dust content (the difference in the extinctions between different lines-of-sight being only $\Delta E(B - V) \simeq 0.2$ mag).

Another potential limitation on the accuracy of lens statistics is uncertainty in the mass evolution of galaxies. Keeton, Kochanek & Falco (1998) and Kochanek et al. (2000) have used lens galaxies to measure the fundamental plane (e.g. Dressler et al. 1997) of field ellipticals at moderate redshifts, but very little could be inferred about the mass evolution of the population. Assuming the present-day population of ellipticals formed from the mergers of spirals (or other smaller halos), the high-redshift deflector population should consist of a larger number of less massive objects. If the total mass in halos is conserved the lensing optical depth is independent of the evolution, but the average image separation is decreased (e.g. Rix et al. 1994). Mao & Kochanek (1994) used this fact to show that the known quasar lenses were best explained if there was little or no evolution in the elliptical population to redshifts of order unity. Thus a non-evolving population of elliptical galaxies is adopted here.

The mass profile of the deflectors has a greater impact on the frequency of multiply-imaged sources, as well as the resultant image configurations. Constant mass-to-light ratio de Vaucouleurs (1948) models of ellipticals can be matched to either the galaxy dynamics (Kormendy & Djorgovski 1989; van der Marel 1991) or lens statistics (Maoz & Rix 1993; Kochanek 1996b), but not to both simultaneously. The mass-to-light ratios required to reproduce the observed image separations are approximately double those suggested by dynamical arguments. This implies that ellipticals are dominated by dark matter halos, which might be expected to follow the Navarro, Frenk & White (1996, 1997) mass profile inferred from N -body simulations of cold dark matter-dominated galaxy formation. However, in the inner regions – which determine the strong lensing properties – this profile is only marginally steeper than the de Vaucouleurs (1948) model, and is inconsistent with lensing observations for the same reasons. The inferred dark matter halos can be modelled as isothermal spheres (e.g. Binney & Tremaine 1987), which are consistent with both dynamical considerations (e.g. Kormendy & Richstone 1995) and lensing data (e.g. Kochanek 1993, 1996b). There is, however, some uncertainty as to the correct mass normalisation of this model (characterised by a velocity dispersion, σ_∞), due to both its relationship with the observed line-of-sight velocity dispersion, $\sigma_{||}$, and the possibility of a finite core. The lensing cross-section of an isothermal galaxy is proportional

to σ_∞^4 (Turner et al. 1984), so even small variations in the normalisation are important.

The surface brightness of ellipticals is flatter than an isothermal profile near the centre (and steeper at large radii, although this is less relevant), which results in higher observed velocity dispersions for a given mass distribution than constant mass-to-light ratio models (e.g. Binney & Tremaine 1987). Gott (1977) used the conversion $\sigma_\infty = (3/2)^{1/2} \sigma_{||}$ to account for the extended nature of the dark matter halo, but more recent calculations imply that the correct scaling is much closer to unity (e.g. Kochanek 1993, 1994). This result is supported by lens statistics (e.g. Kochanek 1996b), but the uncertainties are quite large.

If ellipticals do have finite cores (within which the density is roughly constant), the the maximum deflection angle is reduced, making them less effective lenses (e.g. Hinshaw & Krauss 1987; Blandford & Kochanek 1987). However, the mass normalisation is increased for a given observed $\sigma_{||}$, as the central potential well of the galaxies are shallower; this tends to increase their lensing effectiveness (Kochanek 1996a,b). Further, non-singular lenses tend to produce more highly magnified images (e.g. Blandford & Kochanek 1987), resulting in an increased lensing probability due to magnification bias (Turner 1980). The qualitative arguments are quite clear, but the relative importance of the various effects, and their overall impact on lens statistics, are not.

In Section 2 the normalisation and resultant scalings of the mass distribution are derived, and the effects these have on the optical depth and lensing probability of elliptical galaxies are discussed in Section 3. The conclusions reached on the effect of core radii on lens statistics are then summarised in Section 4.

2 ELLIPTICAL GALAXIES

A simple model for the population of elliptical galaxies (Section 2.1) is adopted here, in which individual galaxies are assumed to be spherically symmetric objects, completely defined by their radial mass distribution (Section 2.2), radial luminosity density (Section 2.3), and dynamics. Given that the line-of-sight velocity dispersion in the central regions is usually used for the dynamical normalisation of ellipticals, this observable must be related to the model parameters for self-consistency (Section 2.4).

2.1 Population

If elliptical galaxies follow a Schechter (1976) luminosity function, and obey the Faber-Jackson (1976) relationship, their local co-moving number density is given by

$$\frac{dn_g}{d\sigma_{||}} = \frac{\gamma n_*}{\sigma_*} \left(\frac{\sigma_{||}}{\sigma_*} \right)^{\gamma(1+\alpha)-1} \exp \left[- \left(\frac{\sigma_{||}}{\sigma_*} \right)^\gamma \right], \quad (1)$$

where $\sigma_{||}$ is the observed line-of-sight velocity dispersion, $\alpha = -1.07 \pm 0.05$ and $n_* = (0.0019 \pm 0.003) h^3 \text{ Mpc}^{-3}$ (Efsthathiou, Ellis & Peterson 1988). Here $H_0 = 100h \text{ km s}^{-1} \text{ Mpc}^{-1}$ is Hubble's constant, and $\sigma_* = 225 \pm 20 \text{ km s}^{-1}$ and $\gamma = 3.7 \pm 1$ (de Vaucouleurs & Olson 1982). There is the possibility of systematic uncertainties in equation (1) for low $\sigma_{||}$ (e.g. Folkes et al. 1999), but the larger galaxies dominate the strong lensing by ellipticals. Further, any scatter

in the Faber-Jackson (1976) relation effectively increases σ_* by an amount comparable to the scatter in $\sigma_{||}$ (Kochanek 1994).

Under the assumption that the galaxy population is non-evolving (See Section 1.), the differential number of galaxies at redshift z and with velocity dispersion $\sigma_{||}$ is

$$\frac{d^2 N_g}{dz d\sigma_{||}} = \frac{dV_0}{dz} \frac{dn_g}{d\sigma_{||}}, \quad (2)$$

where dV_0/dz is the co-moving volume element at redshift z . Its full cosmological dependence is rather complex (e.g. Carroll, Press & Turner 1992; Kayser, Helbig & Schramm 1997) and so only three simple, limiting cases are used here: $\Omega_{m0} = 1$ and $\Omega_{\Lambda 0} = 0$ (the Einstein-de Sitter model); $\Omega_{m0} = 0$ and $\Omega_{\Lambda 0} = 0$ (the empty Milne model); and $\Omega_{m0} = 0$ and $\Omega_{\Lambda 0} = 1$ (a cosmological constant-dominated flat model). In these models the volume element becomes

$$\frac{dV_0}{dz} = \begin{cases} 4\pi \left(\frac{c}{H_0}\right)^3 \frac{4(z+2\sqrt{1+z+2})}{(z+1)^{5/2}}, & \text{if } \Omega_{m0} = 1 \text{ and } \Omega_{\Lambda 0} = 0, \\ 4\pi \left(\frac{c}{H_0}\right)^3 \frac{z^2(z+2)^2}{4(z+1)^3}, & \text{if } \Omega_{m0} = 0 \text{ and } \Omega_{\Lambda 0} = 0, \\ 4\pi \left(\frac{c}{H_0}\right)^3 z^2, & \text{if } \Omega_{m0} = 0 \text{ and } \Omega_{\Lambda 0} = 1. \end{cases} \quad (3)$$

2.2 Mass distribution

Despite its unbounded total mass, the non-singular isothermal sphere is consistent with the dynamics of elliptical galaxies (and their lensing properties). The Hinshaw & Krauss (1987) model has a mass density given by

$$\rho_M(r) = \frac{\sigma_\infty^2}{2\pi G} \frac{1}{(r^2 + r_c^2)}, \quad (4)$$

where r_c is the core radius and σ_∞ is the line-of-sight velocity dispersion away from the core for a constant mass-to-light ratio galaxy. The integrated mass is given by

$$M(<r) = \frac{2\sigma_\infty^2 r_c}{G} \left[\frac{r}{r_c} - \arctan\left(\frac{r}{r_c}\right) \right] \quad (5)$$

and the projected surface density by

$$\Sigma_M(R) = \frac{\sigma_\infty^2}{2G} \frac{1}{\sqrt{R^2 + r_c^2}}, \quad (6)$$

which can also be integrated analytically to give

$$M(<R) = \frac{\sigma_\infty^2}{G} \left(\sqrt{R^2 + r_c^2} - r_c \right). \quad (7)$$

As discussed in Section 2.3, the luminosity density of many ellipticals appears to be effectively singular, but such observations cannot directly constrain the mass distribution. Nonetheless, there are at least two strong arguments to suggest that r_c is small as well. Firstly, most lensed quasars have even numbers of images (e.g. Keeton & Kochanek 1996), which implies that the galaxies' mass distributions are very nearly singular (e.g. Wallington & Narayan 1993; Kassiola & Kovner 1993). Secondly, dynamical modelling, combined with high-resolution *Hubble Space Telescope* imaging of nearby ellipticals, reveals that a number have large black

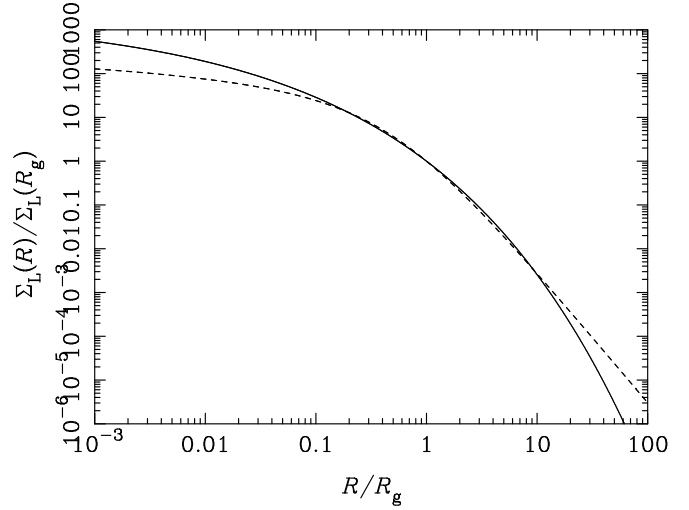


Figure 1. The projected luminosity density of galaxies described by a de Vaucouleurs (1948) law (solid line) and a Hernquist (1990) profile (dashed line), scaled by their values at their effective or half-light radius, R_g .

holes at their centres, and so are formally infinitely dense there (e.g. Kormendy et al. 1996, 1997). If the core radius is non-zero, its scaling with σ is important (Kochanek 1991; Section 3), and is taken to be

$$r_c = r_{c*} \left(\frac{\sigma_{||}}{\sigma_*} \right)^{u_c}, \quad (8)$$

where $u_c = 4 \pm 1$ (e.g. Fukugita & Turner 1991).

2.3 Light distribution

Two models of the surface brightness of ellipticals are used here; both are compatible with observations, and the difference between the results of the two models is an indication of the uncertainty of this calculation.

The first is a de Vaucouleurs (1948) profile, given by

$$\Sigma_L(R) = 296.7 \frac{L}{\pi R_g^2} \exp \left[-7.67 \left(\frac{R}{R_g} \right)^{1/4} \right], \quad (9)$$

where R_g is the effective or half-light radius of the galaxy and L is its luminosity. This is shown in Fig. 1 as the solid line. The luminosity density is given by an Abel integral (Binney & Tremaine 1987) as

$$\rho_L(r) = -\frac{1}{\pi} \int_r^\infty \frac{d\Sigma_L}{dR} \frac{1}{\sqrt{R^2 - r^2}} dR. \quad (10)$$

It must be computed numerically for most r , but can be approximated by $\rho_L(r) \simeq 1096.6 L/(\pi^2 R_g^3) (r/R_g)^{-3/4}$ for $r \rightarrow 0$ (Young 1976).

The second model is based on a Hernquist (1990) profile, which was developed as an analytical approximation to the de Vaucouleurs (1948) profile, but fits the data just as well in its own right. With $R_H \simeq 0.55 R_g$,[†] the surface brightness is

[†] The definition $R_H \simeq 0.45 R_g$ is sometimes used (e.g. Kochanek 1996b), but it is more relevant for the dynamics of constant mass-to-light models than for luminosity profiles alone.

$$\Sigma_L(R) = \frac{L}{2\pi R_H^2} \frac{[2 + (R/R_H)^2] [f_H(R/R_H) - 3]}{[1 - (R/R_H)^2]^2}, \quad (11)$$

where

$$f_H(x) = \begin{cases} \frac{\operatorname{arccosh}(1/x)}{\sqrt{1-x^2}}, & \text{if } x < 1, \\ 1, & \text{if } x = 1, \\ \frac{\arccos(1/x)}{\sqrt{x^2-1}}, & \text{if } x > 1. \end{cases} \quad (12)$$

This is shown as the dashed line in Fig. 1, and is qualitatively similar to the de Vaucouleurs (1948) profile for $0.1R_g \lesssim R \lesssim 10R_g$. The fraction of the flux in the discrepant regions is only a few per cent. The resultant luminosity density is given by

$$\rho_L(r) = \frac{L}{2\pi R_H^3} \frac{1}{r/R_H(1+r/R_H)^3}. \quad (13)$$

The spatial scale of both distributions is determined by the effective radius, which, like the core radius of the mass distribution, is assumed to increase with the velocity dispersion of the galaxy as

$$R_g = R_{g*} \left(\frac{\sigma_{||}}{\sigma_*} \right)^{u_g}, \quad (14)$$

where $R_{g*} = (4 \pm 1)h$ kpc and $u_g = 4 \pm 1$ (Kormendy & Djorgovski 1989).

2.4 Dynamical normalisation

The population of galaxies is given in terms of $\sigma_{||}$ in Section 2.1, but the mass distribution, and hence lensing properties of individual galaxies are determined by σ_∞ (Section 2.2). For a given σ_∞ , the central dispersion decreases with increasing core radius, but also depends on both the stellar dynamics within the galaxy and the luminosity profile. Radial orbits result in higher dispersions, as the stars fall through the core of the galaxy, and more extended luminosity profiles also result in faster central stellar motions. The galaxy model is specified by $\rho_M(r)$ and $\rho_L(r)$, given in Sections 2.2 and 2.3, respectively, and the (assumed constant) velocity anisotropy, β_σ . This is defined as $\beta_\sigma = 1 - \sigma_\theta^2/\sigma_r^2$, where σ_θ , σ_ϕ (which are equal in a non-rotating system) and σ_r are the angular and radial components, respectively, of the velocity dispersion tensor of the luminous matter. Both theoretical and observational results suggest that $0.0 \lesssim \beta_\sigma \lesssim 0.5$ for ellipticals (Binney & Tremaine 1987; van der Marel 1991; Kochanek 1994), but a broader range of values is explored here.

Under the above assumptions, the Jeans equation reduces to (e.g. Binney & Tremaine 1987)

$$\sigma_r^2(r) \left[\frac{2}{\sigma_r(r)} \frac{d\sigma_r}{dr} + \frac{1}{\rho_L(r)} \frac{d\rho_L}{dr} + \frac{2\beta_\sigma}{r} \right] = -\frac{GM(<r)}{r^2}, \quad (15)$$

which can be integrated to give

$$\sigma_r(r) = \left[\frac{r^{-2\beta_\sigma}}{\rho_L(r)} \int_r^\infty GM(<r') \rho_L(r') r'^{2(\beta_\sigma-1)} dr' \right]^{1/2}. \quad (16)$$

This can be found analytically in the regions where ρ_M is purely isothermal and ρ_L can be approximated by a global power law, given by $\rho_L(r) \propto r^{-\xi}$ [and hence $\Sigma_L \propto R^{-(\xi-1)}$,

provided that $\xi > 1$]. The Hernquist (1990) model approaches $\xi = 1$ for small r and $\xi = 4$ for large r ; the de Vaucouleurs (1948) law has $\xi = 3/4$ for small radii. The radial dispersion in these regimes is then

$$\sigma_r(r) = \sigma_\infty \left(\frac{2}{\xi - 2\beta_\sigma} \right)^{1/2}. \quad (17)$$

In the outer regions the core radius has no effect, but for $r \lesssim r_c$ the lowered central density is more important than both ρ_L and the velocity anisotropy (assuming $\beta_\sigma \lesssim 0.5$). If $\beta_\sigma \simeq 1$, the orbits are predominantly radial, and luminous material ‘plunges’ through the central regions of the galaxy, greatly increasing σ_r .

The line-of-sight velocity dispersion at a given position on the galaxy is given by a projection integral (e.g. Binney & Tremaine 1987) as

$$\sigma_{||}(R) = \left[\frac{2}{\Sigma_L(R)} \int_R^\infty \frac{(1 - \beta_\sigma R^2/r^2)r}{\sqrt{r^2 - R^2}} \rho_L(r) \sigma_r^2(r) dr \right]^{1/2}. \quad (18)$$

The power law approximations discussed above are also valid here; insertion of equation (17) into the integral yields

$$\sigma_{||}(R) = \sigma_\infty \left[\frac{2}{\xi - 2\beta_\sigma} \frac{\xi - (\xi - 1)\beta_\sigma}{\xi} \right]^{1/2}. \quad (19)$$

In the special case of $\xi = 3$, the standard result (Gott 1977), valid for all β_σ , that $\sigma_{||}(R) = (2/3)^{1/2} \sigma_\infty$, is recovered. It is also clear that the line-of-sight dispersion is lower in regions with a steeper luminosity density. Fig. 2 shows $\sigma_{||}/\sigma_\infty$ as a function of R for the de Vaucouleurs (1948) and Hernquist (1990) models. For both singular models and those with $\beta_\sigma \simeq 1$, the central dispersion results is much higher than the dispersions at large radii. Conversely, the central dispersion decreases with core radius, as the galaxy’s gravitational well is shallower, and bound orbits must be slower. Again the core radius is more important than the anisotropy of luminosity profile, provided only that $\beta_\sigma \lesssim 0.5$.

A real velocity dispersion is measured from a spectrum taken over a finite region of the galaxy, in the form of either a linear slit or, more commonly now, an optical fibre. Assuming a circular aperture of projected radius R_f centred on the galaxy, the observed line-of-sight velocity dispersion is

$$\sigma_{||}(< R_f) = \frac{\int_0^{R_f} 2\pi R \Sigma_L(R) \sigma_{||}(R) dR}{\int_0^{R_f} 2\pi R \Sigma_L(R) dR}. \quad (20)$$

Atmospheric seeing would have the effect of smoothing the function $\sigma_{||}(R)$, but its importance is minimal as this tends to be a slowly varying function for $R \gtrsim R_g$. For a fixed angular size, θ_f , the aperture will vary from galaxy to galaxy as $R_f = d_A(0, z)\theta_f \simeq cz\theta_f/H_0$, where $z \ll 1$ is the galaxy’s redshift, and d_A its the angular diameter distance. Only nearby galaxies are practical targets for dynamical studies – for instance the samples of van der Marel (1991) and Lauer et al. (1995) contain galaxies with $0.002 \lesssim z \lesssim 0.02$ and $0.0006 \lesssim z \lesssim 0.06$, respectively. Hence an aperture a few arcsec in diameter implies $0.01 \text{ kpc} \lesssim R_f \lesssim 1 \text{ kpc}$, as compared to core radii of $\sim 0.1 \text{ kpc}$ and effective radii of $\simeq 4 \text{ kpc}$. Figs. 3 and 4 show the normalisation for singular models as a function of R_f and β_σ , respectively. The

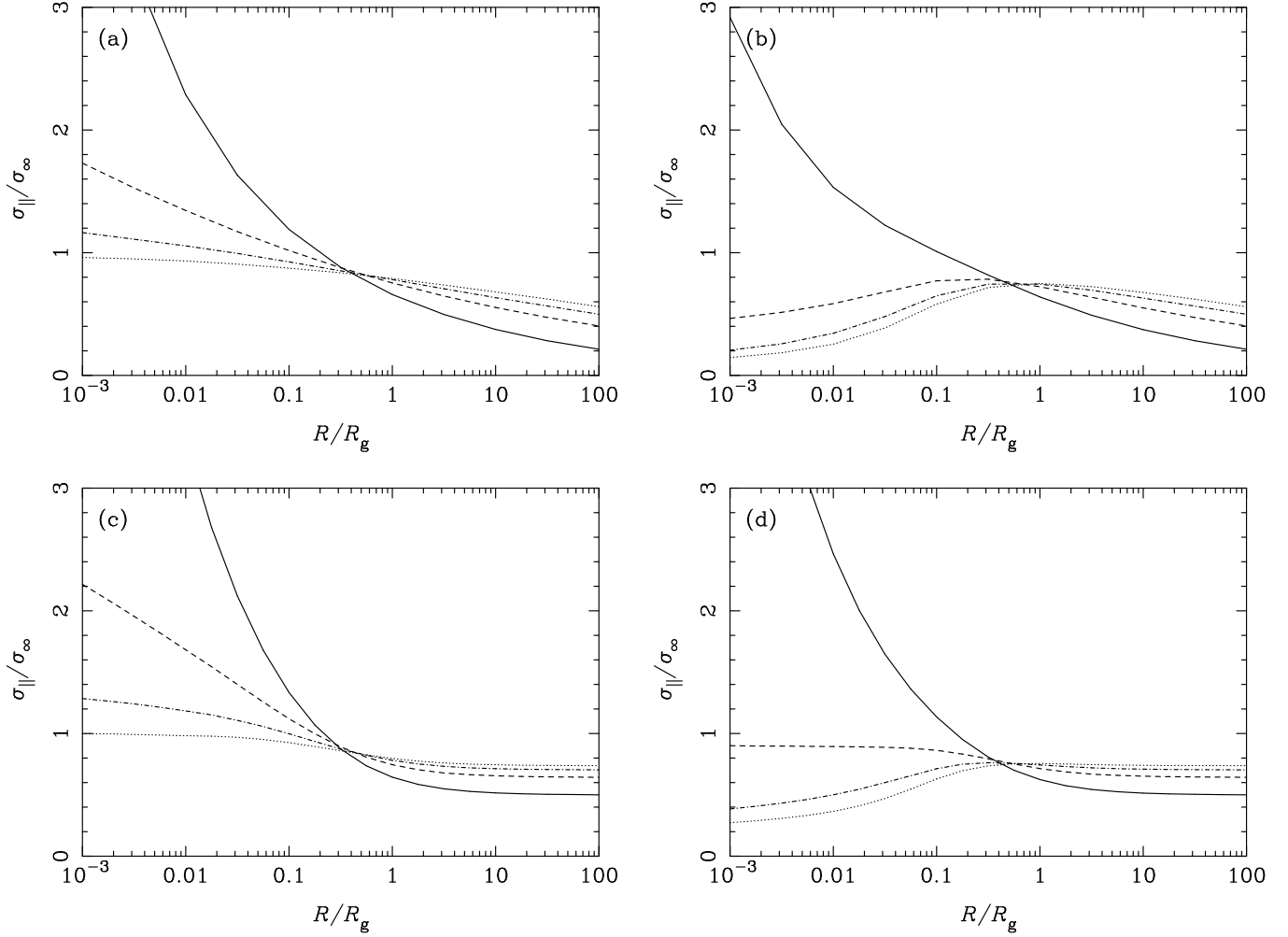


Figure 2. The line-of-sight velocity dispersion, $\sigma_{||}$, of the luminous matter in an elliptical galaxy with luminosity densities described by a de Vaucouleurs (1948) law in (a) and (b) and a Hernquist (1990) model in (c) and (d). In (a) and (c) the mass distribution is a singular isothermal sphere; in (b) and (d) it has a core radius of $0.1R_g$, where R_g is the effective radius of the galaxy. The four lines in each panel represent different values of the velocity anisotropy: $\beta_\sigma = 1.0$ (solid lines); $\beta_\sigma = 0.5$ (dashed lines); $\beta_\sigma = 0.0$ (dot-dashed lines); and $\beta_\sigma = -0.5$ (dotted lines). The regions where $\sigma_{||}$ is flat are those where the luminosity density can be approximated as a global power law.

normalisation increases with R_f as the observed dispersion is less dependent on the extreme orbital speeds near the core. Conversely, the normalisation decreases with β_σ , as the maximum orbital speeds are higher for radial orbits. Fig. 5 shows $\sigma_\infty/\sigma_{||}(< R_f)$ as a function of core radius. The general trend is that the observed velocity dispersion decreases (and so the dynamical normalisation increases) with core radius and also with R_f . It is also clear that the quantitative behaviour varies comparably with the dynamical model and luminosity density assumed. For smaller apertures this dependence is more extreme, as only the core region is directly observed.

Calculation of $\sigma_{||}(< R_f)$ is computationally expensive, especially for the de Vaucouleurs (1948) model; fortunately its dependence on core radius is very nearly linear. For the subsequent lens calculations, the normalisation used is

$$\sigma_\infty = \sigma_{||}(< R_f) \left(A + B \frac{r_c}{R_g} \right), \quad (21)$$

where A and B independent of core radius. Kochanek

(1996b) used $A = 1$ and $B = 2$ for galaxies with $R_f \simeq R_g$, but this underestimates the normalisation by up to ~ 15 per cent (See Fig. 5.), and hence underestimates the lensing probability by up to ~ 80 per cent. As defined above, A is determined purely by the singular models, for which the normalisation is plotted in Figs. 3 and 4. Also, A should match the power-law approximation given by equation (19) for very small apertures, and $\sigma_\infty/\sigma_{||}(< R_f) \rightarrow (3/2)^{1/2} \simeq 1.225$ for $R_f \rightarrow \infty$, as shown by Kochanek (1993). For intermediate apertures, the variation between the results for the two luminosity profiles can be used as a guide to the uncertainty in the above results. Given this discrepancy, analytical expressions for A and B were developed for both the de Vaucouleurs (1948) and Hernquist (1990) profiles, and these were used in the lensing calculations presented in Section 3. The analytical forms are given in Mortlock (1999), and, for all reasonable galactic models, agree with the numerical results to within a few per cent; the uncertainty in the normalisation caused by the ambiguity in the choice of

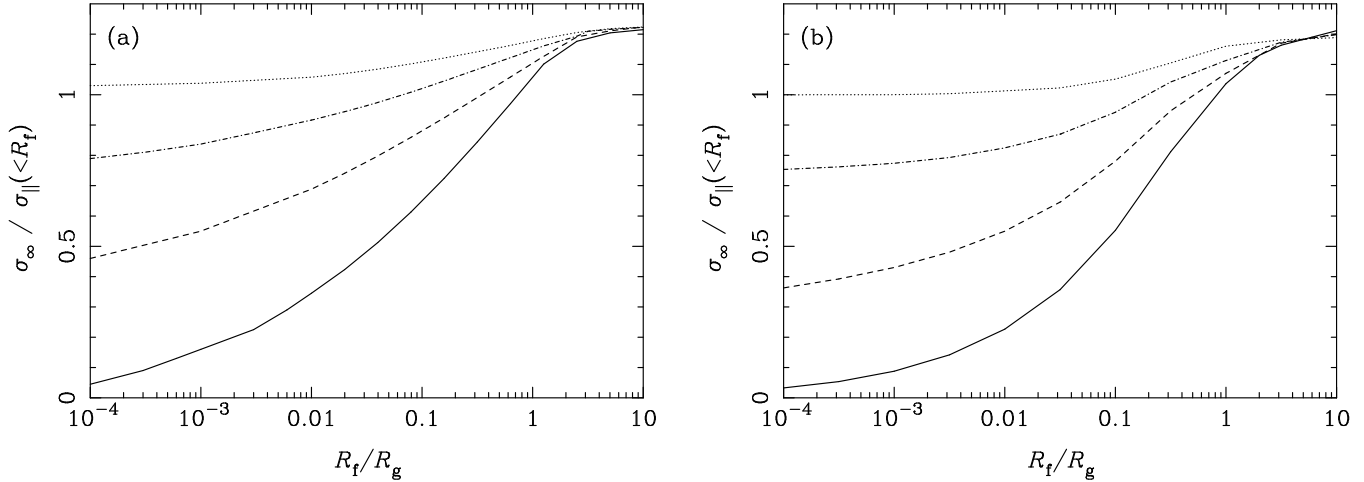


Figure 3. The dynamical normalisation, σ_∞ , as a function of the size of the integration aperture, R_f , for a singular galaxy with effective radius R_g and observed line-of-sight velocity dispersion σ_\parallel . The luminosity density is described by a de Vaucouleurs (1948) law in (a) and a Hernquist (1990) model in (b). Different values of the velocity anisotropy are denoted by the different line-styles: $\beta_\sigma = 1.0$ (solid lines); $\beta_\sigma = 0.5$ (dashed lines); $\beta_\sigma = 0.0$ (dot-dashed lines); and $\beta_\sigma = -0.5$ (dotted lines).

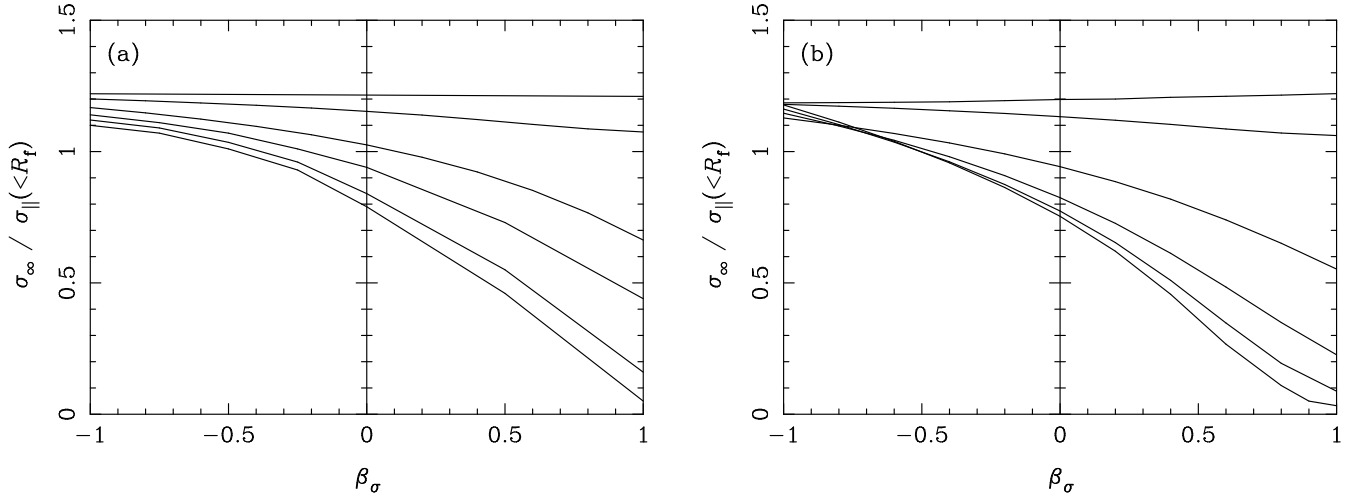


Figure 4. The dynamical normalisation, σ_∞ , as a function of the velocity anisotropy, β_σ , for a singular galaxy with effective radius R_g and observed line-of-sight velocity dispersion σ_\parallel . The luminosity density is described by a de Vaucouleurs (1948) law in (a) and a Hernquist (1990) model in (b). The lines represent different aperture sizes – from the bottom to the top, R_f/R_g takes on the values: 0.0001, 0.001, 0.01, 0.1, 1.0 and 10.0.

luminosity profile is considerably larger at around 10 per cent.

Having found a relationship between the isothermal mass normalisation and observables for a given galaxy, there still remains the question of how best to make the conversion from the observed Faber-Jackson (1976) relation. A ‘natural’ choice is to consider the aperture to be a specified fraction of the effective radius of each galaxy in the sample although this is unrealistic for large surveys undertaken using fibres of a fixed radius. (However, if the data is available, it is preferable to measure the velocity dispersion out to $\sim R_g$, as the results are more robust.) The other possibility is to treat measured dispersions as being averaged over a given physical scale, independent of σ_\parallel , but this breaks down for small galaxies as only the central regions are likely to be registered due to surface brightness considerations. One way to circum-

vent these ambiguities is to fit the mass model directly from dynamical measurements on a galaxy-by-galaxy basis (e.g. van der Marel 1991; Kockanek 1994). This is not only more time-consuming, but also requires spatially resolved surface brightness and velocity dispersion measurements.

The ‘default’ model ($\beta_\sigma = 0$; $R_f \simeq R_g$; $r_c = 0$) has $\sigma_\infty/\sigma_\parallel \simeq 1.1$, leading to a 50 per cent increase in the lensing probability, due to its σ_∞^4 dependence (e.g. Turner et al. 1984; Kochanek 1994). For most of the other plausible sets of parameter values the differences are even greater. Similar increases in the lensing probability can also result from the spread in the Faber-Jackson (1976) relation – a dispersion of $\Delta\sigma_\infty/\sigma_\infty \simeq 0.2$ increases the lensing optical depth (Section 3.2) by a factor of $\sim 1 + 6(\Delta\sigma_\infty/\sigma_\infty)^2 \simeq 1.25$ (Kochanek 1994). If a number of other common simplifications used in lensing calculations are correct (e.g. that

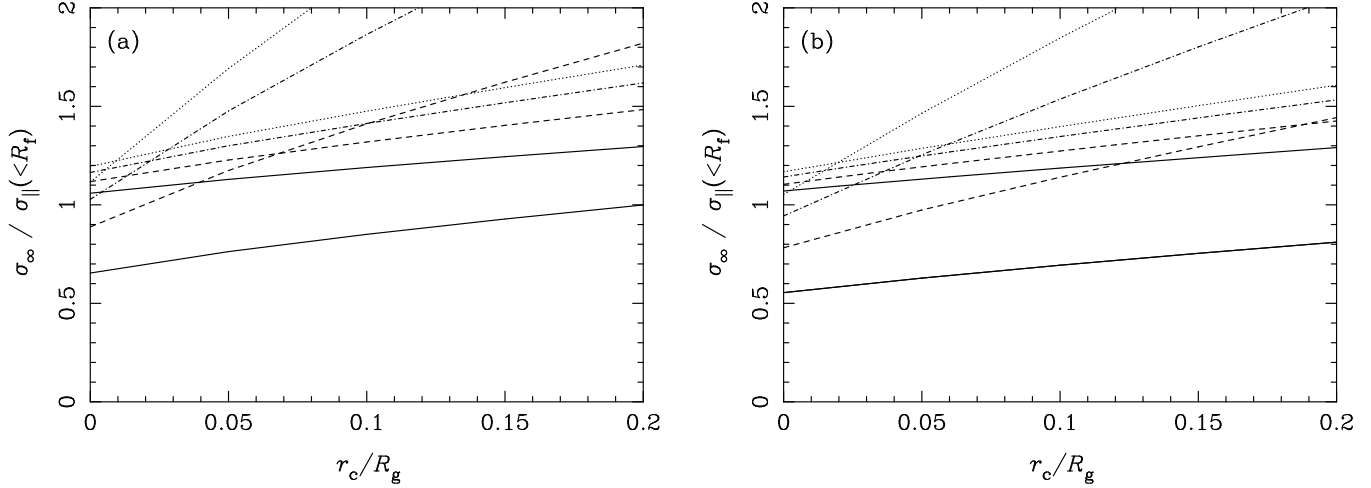


Figure 5. The dynamical normalisation, σ_∞ , as a function of core radius, r_c , for a galaxy with effective radius R_g and observed line-of-sight velocity dispersion $\sigma_{||}$. The luminosity density is described by a de Vaucouleurs (1948) law in (a) and a Hernquist (1990) model in (b). Different values of the velocity anisotropy are denoted by the different line-styles: $\beta_\sigma = 1.0$ (solid lines); $\beta_\sigma = 0.5$ (dashed line); $\beta_\sigma = 0.0$ (dot-dashed lines); and $\beta_\sigma = -0.5$ (dotted lines). The two lines for each dynamical model are for different values of the aperture size: $R_f = 0.1 R_g$; and $R_f = R_g$. The larger projected fibre radius results in less variation between dynamical models and higher values of σ_∞ for $r_c = 0$, but lower values of σ_∞ if the core radius is large.

spiral galaxies are unimportant; that obscuration by dust is minimal; etc.), the dynamical normalisation is probably the greatest uncertainty in lens statistics at present. Further, whereas uncertainty in n_* can be greatly decreased by simple counting procedures, accurate normalisation (or, equivalently, measurement of $d n_g / d \sigma_\infty$) requires much more detailed data.

3 LENSING PROBABILITY

From the introduction of finite cores to lens galaxies by Hinshaw & Krauss (1987) it was generally believed that the fraction of quasars which are multiply-imaged drops sharply with increasing core radius. However as shown by Kochanek (1996a,b) the requirements of self-consistent dynamical normalisation (Section 2.4) imply that the lensing probability declines only slowly, or possibly even increases with core radius. Once the lens equation has been solved (Section 3.1), these possibilities are quantified in terms of both the optical depth (Section 3.2) and a simple but self-consistent calculation of lensing probability of a distant quasar (Section 3.3).

3.1 The lens equation

The lens equation relates the angular position (relative to the optical axis joining the observer and the centre of the lens) of the source, β , to those of its image(s), θ . These quantities can only be related via $d_A(0, z_d)$, $d_A(0, z_s)$ and $d_A(z_d, z_s)$, the angular diameter distances from observer to deflector, observer to source, and deflector to source, respectively. In the filled-beam approximation (Dyer & Roeder 1972, 1973), the angular diameter distances in the cosmological models described in Section 2.1 are given by

$$d_A(z_1, z_2) = \quad (22)$$

$$\begin{cases} \frac{c}{H_0} \frac{2}{z_2+1} \left(\frac{1}{\sqrt{z_1+1}} - \frac{1}{\sqrt{z_2+1}} \right), & \text{if } \Omega_{m0} = 1 \text{ and } \Omega_{\Lambda0} = 0, \\ \frac{c}{H_0} \frac{z_2(z_2+2) - z_1(z_1+2)}{2(z_1+1)(z_2+1)^2}, & \text{if } \Omega_{m0} = 0 \text{ and } \Omega_{\Lambda0} = 0, \\ \frac{c}{H_0} \frac{z_2 - z_1}{z_2 + 1}, & \text{if } \Omega_{m0} = 0 \text{ and } \Omega_{\Lambda0} = 1. \end{cases}$$

For a thin lens with a cumulative surface mass distribution $M(< R)$, standard techniques (e.g. Schneider, Ehlers & Falco 1992) give the lens equation as

$$\beta = \theta - \frac{1}{\pi \theta} \frac{M[< d_A(0, z_d) \theta]}{d_A^2(0, z_d) \Sigma_{\text{crit}}(z_d, z_s)}, \quad (23)$$

where

$$\Sigma_{\text{crit}}(z_d, z_s) = \frac{c^2}{4\pi G} \frac{d_A(0, z_s)}{d_A(0, z_d) d_A(z_d, z_s)} \quad (24)$$

is the surface density required for a rotationally-symmetric lens to be capable of forming multiple images (e.g. Subramanian & Cowling 1986; Schneider et al. 1992).

Using the mass distribution given in equation (7), the lens equation becomes

$$\beta = \theta - \theta_E \frac{\sqrt{1 + \theta^2 / \theta_c^2} - 1}{\theta / \theta_c}. \quad (25)$$

where $\theta_c = r_c / d_A(0, z_d)$ and

$$\theta_E = 4\pi \left(\frac{\sigma_\infty}{c} \right)^2 \frac{d_A(z_d, z_s)}{d_A(0, z_s)} \quad (26)$$

is the Einstein angle[†] of the singular ($r_c = 0$) lens. The dynamical normalisation, σ_∞ , is given in terms of observables in Section 2.4.

[†] If the source, lens and observer are colinear, a circular image is formed. The angular radius of this circle is the Einstein angle.

Equation (25) and ‘a little algebra’ (Hinshaw & Krauss 1987) give

$$\begin{aligned} 0 &= \theta^3 - 2\beta\theta^2 + (\beta^2 + 2\theta_E\theta_c - \theta_E^2)\theta - 2\theta_E\theta_c\beta \\ &= \left(\theta - \frac{2}{3}\beta\right)^3 - 3p\left(\theta - \frac{2}{3}\beta\right) - 2q, \end{aligned} \quad (27)$$

where $p = (3\theta_E^2 + \beta^2 - 6\theta_E\theta_c)/9$ and $q = \beta(9\theta_E^2 + 9\theta_E\theta_c - \beta^2)/27$. There are three solutions for θ if $q^2 < p^3$, two if $q^2 = p^3$ and only one if $q^2 > p^3$. Note that not all solutions need not correspond to image positions, as equation (27) is not strictly equivalent to equation (25).

If $\theta_c > \theta_E/2$, equation (27) can have only ever have one solution, as the central surface density of the lens is less than Σ_{crit} [equation (24)]. However, all but the most nearby galaxies have $\theta_c < \theta_E/2$ and so can form multiple images. In this case, expanding p and q , and disregarding multiple solutions that do not correspond to images, yields the result that a source is multiply-imaged is $\beta \leq \beta_{\text{crit}} = \beta_-$, where

$$\beta_{\pm} = \begin{cases} \left[\theta_E^2 + 5\theta_E\theta_c - \frac{1}{2}\theta_c^2 \pm \frac{1}{2}\sqrt{\theta_c(\theta_c + 4\theta_E)^3} \right]^{1/2}, & \text{if } \theta_c < \theta_E/2, \\ 0, & \text{if } \theta_c \geq \theta_E/2. \end{cases} \quad (28)$$

If $r_c = 0$, the lens is always critical, and $\beta_{\text{crit}} = \theta_E$. The cross-section for multiple-imaging is then simply $\pi\beta_{\text{crit}}^2$, but the image positions and magnifications are needed for the more realistic lensing calculation (Section 3.3). If $\theta_c \ll \theta_E$ and $\sigma_{||}$ is fixed, β_{crit} decreases slowly with core radius, as there is little increase in σ_{∞} . For larger core radii, however, σ_{∞} increases nearly linearly with r_c , so, from equation (26), $\beta_{\text{crit}} \propto \theta_E \propto r_c^2$. Hence β_{crit} eventually increases with core radius. For large galaxies this only occurs for unrealistically large values of r_c , but it can come into effect for very small galaxies if the fibre integration area is small (Section 3.2).

If $(0 \leq) \beta \leq \beta_{\text{crit}}$, the source is lensed, and the three images are located at

$$\theta_i(\beta) = \frac{2}{3}\beta + 2\sqrt{p} \cos \left[\frac{1}{3} \arccos \left(\frac{q}{\sqrt{p^3}} \right) + \frac{2i\pi}{3} \right], \quad (29)$$

where $i = 1, 2$ or 3 , and two of the images are coincident if $\beta = \beta_{\text{crit}}$. Note that this formula breaks down if the lens is singular, in which case only two images are formed. They are located at $\theta_1 = \beta + \theta_E$ and $\theta_2 = \beta - \theta_E$. To within 10 per cent, the angular separation between the outer pair of images is independent of source position, and is given by (Hinshaw & Krauss 1987)

$$\Delta\theta \simeq \begin{cases} 0, & \text{if } \theta_c > \theta_E/2, \\ \theta_E \sqrt{1 - 2\theta_c/\theta_E}, & \text{if } \theta_c \leq \theta_E/2. \end{cases} \quad (30)$$

This expression becomes exact in the singular case.

If $\beta > \beta_{\text{crit}}$, the source is unlensed, and there is only one image. For the range $\beta_{\text{crit}} = \beta_- < \beta \leq \beta_+$ the single image position is

$$\theta(\beta) = \frac{2}{3}\beta + \left(q - \sqrt{q^2 - p^3}\right)^{1/3} + p \left(q - \sqrt{q^2 - p^3}\right)^{-1/3}. \quad (31)$$

If $\beta > \beta_+$, equation (27) has three solutions, two of which do not represent image positions. The one solution that does is

$$\theta(\beta) = \frac{2}{3}\beta + 2\sqrt{p} \cos \left[\frac{1}{3} \arccos \left(\frac{q}{\sqrt{p^3}} \right) \right]. \quad (32)$$

Again the singular case is much simpler: if $\beta > \theta_E$, the single image is located at $\theta = \beta + \theta_E$.

The lens mapping (from θ to β , or image to source) changes the area subtended by an object; this manifests itself as an increase or decrease in flux, as surface brightness is conserved by gravitational lensing. The area change is given by the Jacobian of the mapping, and so the magnification is the reciprocal of this. For spherically-symmetric lenses (See Schneider et al. 1992.) the magnification of a point source is given by

$$\mu(\theta) = \left| \frac{\beta}{\theta} \frac{\partial\beta}{\partial\theta} \right|. \quad (33)$$

Equation (25) then gives

$$\begin{aligned} \mu(\theta) &= \left| \frac{\theta^2}{\theta^2 + \theta_E\theta_c - \theta_E\sqrt{\theta^2 + \theta_c^2}} \right| \\ &\times \left| \frac{\theta^2\sqrt{\theta^2 + \theta_c^2}}{\theta_E\theta_c^2 + (\theta^2 - \theta_E\theta_c)\sqrt{\theta^2 + \theta_c^2}} \right|. \end{aligned} \quad (34)$$

This expression breaks down for small θ if $\theta_c < \theta_E/2$, but a Taylor expansion about $\theta = 0$ gives

$$\mu(\theta) \simeq \frac{4\theta_c^2/\theta_E^2}{(2\theta_c/\theta_E - 1)^2 + (2\theta_c/\theta_E - 1)\theta^2/\theta_c^2}, \quad (35)$$

for $\theta \ll \theta_E$. If $r_c = 0$, equation (34) reduces to $\mu(\theta) = |\theta/(\theta - \theta_E)|$.

The total magnification of a source is simply the sum of the magnification of its images, and is thus

$$\mu_{\text{tot}}(\beta) = \sum_i \mu[\theta_i(\beta)]. \quad (36)$$

The flux ratio is less well-defined, due to potential presence of three images and observational effects (e.g. Kassiola & Kovner 1993). For three image configurations it is taken to be the flux ratio of the two brightest images.

3.2 Optical depth

The lensing optical depth, τ , as introduced by Turner et al. (1984), is the fraction of the source plane within which the lens equation has multiple solutions. It is a useful estimate of the lensing probability that is independent of observational restrictions and the source luminosity function. In the filled-beam approximation, the contribution to the optical depth by any one lens galaxy, τ_g , is the fraction of the sky covered by its cross-section. Hence $\tau_g = \pi\beta_{\text{crit}}^2/(4\pi)$, with β_{crit} given in equation (28). The optical depth is given by integrating τ_g over the population of deflectors, under the assumption that the individual cross-sections do not overlap. For a source at redshift z_s ,

$$\tau(z_s) = \int_0^{z_s} \int_0^\infty \frac{d^2 N_g}{dz_g d\sigma_{||}} \tau_g d\sigma_{||} dz_g. \quad (37)$$

If the lenses are singular and $\sigma_{\infty} = \sigma_{||}$ is assumed, $\tau_g = \theta_E^2/4$ and the integrals can be performed analytically (e.g. Turner

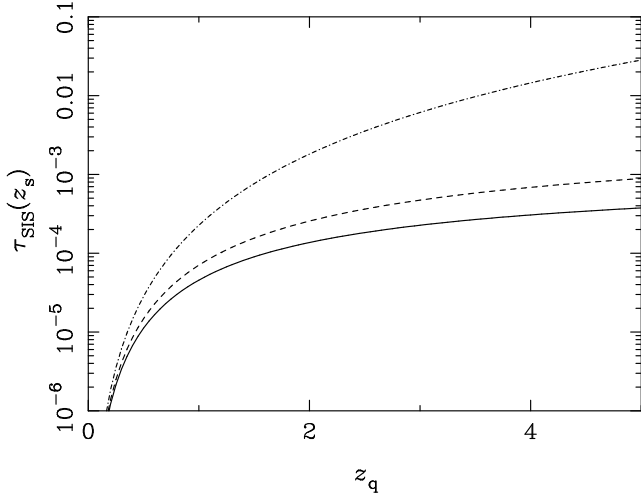


Figure 6. The ‘standard’ lensing optical depth, τ_{SIS} , as a function of source redshift, z_s . This results from a population of singular isothermal spheres with $\sigma_\infty = \sigma_{||}$, and the default parameters described in Section 2. Three cosmological models are shown: $\Omega_{m0} = 1$ and $\Omega_{\Lambda0} = 0$ (solid line); $\Omega_{m0} = 0$ and $\Omega_{\Lambda0} = 0$ (dashed line); and $\Omega_{m0} = 0$ and $\Omega_{\Lambda0} = 1$ (dot-dashed line).

et al. 1984; Schneider et al. 1992; Krauss & White 1992; Kochanek 1993) to give

$$\tau_{\text{SIS}}(z_s) = 16\pi^3 n_* \left(\frac{c}{H_0}\right)^3 \left(\frac{\sigma_{||}}{c}\right)^4 \Gamma\left(1 + \alpha + \frac{4}{\gamma}\right) \quad (38)$$

$$\times \begin{cases} \frac{4}{15} \left(1 - \frac{1}{\sqrt{z_s+1}}\right)^3, & \text{if } \Omega_{m0} = 1 \text{ and } \Omega_{\Lambda0} = 0, \\ \frac{2(z_s^4 + 4z_s^3 + 10z_s^2 + 12z_s + 6) \ln(z_s+1) - 3z_s(z_s+2)(z_s^2 + 2z_s + 2)}{8z_s^2(z_s+2)^2}, & \text{if } \Omega_{m0} = 0 \text{ and } \Omega_{\Lambda0} = 0, \\ \frac{1}{30} z_s^3, & \text{if } \Omega_{m0} = 0 \text{ and } \Omega_{\Lambda0} = 1, \end{cases}$$

where equations (1), (2), (3), (22) and (26) have been used. The prefactor is the same as the F -parameter introduced by Turner et al. (1984) to scale the lensing effectiveness of a galaxy population; for the elliptical galaxy population described in Section 2.1, $F = 0.008 \pm 0.002$. Fig. 6 shows $\tau_{\text{SIS}}(z_s)$ for the three cosmological models, showing the expected increase with redshift as well as the strong dependence on $\Omega_{\Lambda0}$.

The optical depth (normalised to the above analytic cases) is shown as a function of core radius in Fig. 7. Independent of cosmology, the linear conversion $\sigma_\infty \simeq 1.1\sigma_{||}$ results in $\tau/\tau_{\text{SIS}} \simeq 1.5$; if the conversion is $\sigma_\infty \simeq 1.2\sigma_{||}$, then $\tau/\tau_{\text{SIS}} \simeq 2.1$, and the optical depth is doubled. The lower set of lines in Fig. 7 show the marked decrease in τ with core radius that was first demonstrated by Hinshaw & Krauss (1987). The upper set of lines use the normalisation described in Section 2, and show not only the higher optical depth for singular models, but a very different dependence on core radius. For large r_c , the effects of the normalisation becomes very important, and ‘small’ galaxies (with $\sigma_{||} \ll \sigma_*$) dominate the optical depth as their measured dispersion is purely that in the under-dense core. The up-turn in τ is not necessarily realistic, and occurs for core radii that are greater than observed – Kochanek (1996b) found

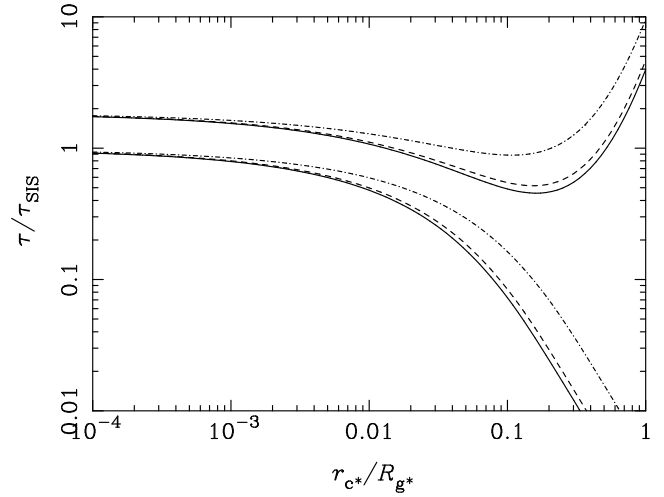


Figure 7. The lensing optical depth, τ , of a source at $z_s = 2$, scaled by the ‘standard’ lensing optical depth for a population of singular isothermal spheres with $\sigma_\infty = \sigma_{||}$. Three cosmological models are shown: $\Omega_{m0} = 1$ and $\Omega_{\Lambda0} = 0$ (solid lines); $\Omega_{m0} = 0$ and $\Omega_{\Lambda0} = 0$ (dashed lines); and $\Omega_{m0} = 0$ and $\Omega_{\Lambda0} = 1$ (dot-dashed lines). The lower set of lines are for $\sigma_\infty = \sigma_{||}$. The values of the other parameters are taken to be: $\beta_\sigma = 0$; $u_c = 4$; $u_g = 4$; and $R_t = R_g$.

$r_c \leq 0.08R_g$ at 95 per cent confidence. For moderate core radii the normalisation is still important – in the $\Omega_{m0} = 0$ and $\Omega_{\Lambda0} = 1$ cosmology, $\tau/\tau_{\text{SIS}} \gtrsim 1$ for all values of r_c . It is also potentially important that a finite core radius actually enhances the cosmological dependence of τ , as most of the lenses are at high-redshift if $\Omega_{\Lambda0} > 0$ (Kochanek 1992).

The dependence of τ on the various galaxy population parameters is shown in Mortlock (1999), but there is little difference between the resultant plots and those shown in Fig. 9 for the quasar lensing probability, and so the optical depth plots are omitted here.

3.3 Quasar lensing probability

The optical depth is a useful measure of lensing likelihood, but it cannot be directly compared to measured lensing frequencies. Hence the probability that a quasar is observed to be lensed, p_q , must be calculated. In the case of the generic lens survey, all the quasars in a parent survey are re-examined for secondary lensed images. Under these conditions, p_q is the fraction of all redshift z_q quasars of magnitude m_q (as measured in the parent survey) that would be revealed as lenses if examined with the resolution and sensitivity of the secondary search. The resolution limit implies a minimum image separation, $\Delta\theta_{\min}$, and the depth of the follow-up observations leads to a maximum magnitude difference between the primary and secondary images, Δm_{\max} . In general there is also a maximum image separation, $\Delta\theta_{\max}$, defined by the extent of the search for companion images.

Most lensed sources are magnified by a factor of 2 or more, so the number of lenses at magnitude m_q is determined by the quasar number counts at least one magnitude fainter. The quasar luminosity function is so steep that this magnification bias (Turner 1980) can double or triple the es-

timated lensing probability. The quasar luminosity function is taken to satisfy

$$\frac{d^2 N_q}{dz dm} \propto \frac{1}{10^{-\alpha_q(m-m_{q0})} - 10^{-\beta_q(m-m_{q0})}} \quad (39)$$

at all redshifts, where $m_{q0} = 19.0 \pm 0.2$ is the magnitude of the break in the number counts, $\alpha_q = 0.9 \pm 0.1$ is the bright-end slope, $\beta_q = 0.3 \pm 0.1$ is the faint-end slope (Boyle, Shanks & Peterson 1988; Kochanek 1996b), and the normalisation unimportant.

The probability a quasar is lensed by a particular galaxy is given by integrating over the source position as (e.g. Kochanek 1995, 1996b)

$$p_{q,g} = \frac{\int_0^{\beta_{\text{crit}}} 2\pi\beta S(\beta) \left. \frac{d^2 N_q}{dz_q dm} \right|_{m=m_q+5/2 \log[\mu_{\text{tot}}(\beta)]} d\beta}{4\pi \frac{d^2 N_q}{dz_q dm_q}}, \quad (40)$$

where $S(\beta)$ is the selection function. It can be approximated by

$$S(\beta) = H[\Delta m_{\text{max}} - \Delta m(\beta)] \times H[\Delta\theta(\beta) - \Delta\theta_{\text{min}}] H[\Delta\theta_{\text{max}} - \Delta\theta(\beta)], \quad (41)$$

where $H(x)$ is the Heavyside step function. Hence $S(\beta) = 1$ if the images of a source at position β satisfy the resolution and sensitivity limits, and is zero otherwise. The use of $\mu_{\text{tot}}(\beta)$ [given in equation (36)] in the calculation of the magnification bias implies that the all the images of the source were unresolved in the parent survey[§], and the pre-factor converts the expression from the surface density of lenses to the fraction of quasars which are lensed.

Integrating $p_{q,g}$ over the deflector population yields (c.f. Kochanek 1996b)

$$p_q = \int_0^{z_q} \int_0^\infty \frac{dV_0}{dz_g} \frac{dn_g}{d\sigma_{||}} p_{q,g} d\sigma_{||} dz_g. \quad (42)$$

This is somewhat simpler for the standard singular lens models (e.g. Kochanek 1993), but no closed form expression for p_q is available unless a simpler form of the quasar luminosity function is used as well.

Fig. 8 shows the probability that an $m_q = 19$ quasar is observed to be lensed by an elliptical galaxy as a function of source redshift. The survey parameters chosen are $\Delta\theta_{\text{min}} = 1$ arcsec, $\Delta\theta_{\text{max}} \rightarrow \infty$ [¶] and $\Delta m_{\text{max}} = 3$. These values affect the overall probability considerably (e.g. Schneider et al. 1992), but do not strongly influence the relative dependence on the other parameters. The lens probability is consistently a factor of ~ 2 higher than the optical depth shown in Fig. 6. Although some lenses are lost due to the angular separation cut-off, many more are magnified into the survey. As with the optical depth, p_q is strongly-dependent on the cosmological model – the similarity of Figs. 6 and 8 demonstrates the generic nature of the cosmological dependence.

[§] This is almost always a valid assumption in the case of galactic lenses, but can result in a serious over-estimate of the magnification bias for more massive deflectors (Mortlock & Webster 2000a).

[¶] Galactic lenses are incapable of producing image separations of more than a few arcsec, so $\Delta\theta_{\text{max}}$ is usually unimportant.

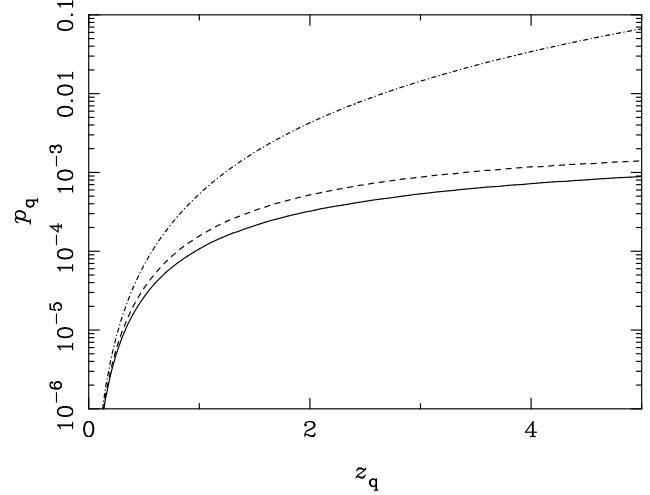


Figure 8. The probability that a $m_q = 19$ quasar at redshift z_q is observed to be multiply-imaged, assuming that all secondary images brighter than $m = 22$ and separated by ≥ 1 arcsec from the primary are found. This results from a population of singular isothermal spheres with $\sigma_\infty = \sigma_{||}$, and the default population parameters described in Section 2. Three cosmological models are shown: $\Omega_{m0} = 1$ and $\Omega_{\Lambda 0} = 0$ (solid line); $\Omega_{m0} = 0$ and $\Omega_{\Lambda 0} = 0$ (dashed line); and $\Omega_{m0} = 0$ and $\Omega_{\Lambda 0} = 1$ (dot-dashed line).

Fig. 9 shows the dependence of p_q on various galaxy population parameters. Firstly, Fig. 9 (a) shows the variation of lensing probability with core radius, in analogy with the optical depth dependence shown in Fig. 7. In the case of the unnormalised model (the single solid line), the high- r_{c*} cut-off is even more pronounced than for τ , despite the effects of the magnification bias. This occurs as the image separation drops below $\Delta\theta_{\text{min}}$ quite quickly. For the correctly normalised models (the set of three lines), the enhancement in p_q is even greater than that for the optical depth (Fig. 7). This comes about both due to the magnification bias and the increased deflection angles of the smaller deflectors. The increase in $\Delta\theta$ for a given $\sigma_{||}$ is another important effect of the dynamical normalisation.

Fig. 9 (b) shows that the velocity anisotropy, β_σ is not as important as the core radius in lens statistics. Whilst the difference between $\beta_\sigma = -1$ and $\beta_\sigma = 1$ can be a factor of several, most results suggest that $\beta_\sigma \simeq 0$ for ellipticals, as discussed in Section 2.4. The lensing probability decreases with β_σ as the observed dispersion within a fixed mass distribution increases with the dominance of radial orbits.

The variation of core radius and effective radius with velocity dispersion is usually unimportant in lensing calculations, as illustrated by the flat parts of the curves in Fig. 9 (c) and (d) as well as Krauss & White (1992). However, in some situations, the values of u_c and u_g [as defined in equations (8) and (14), respectively] can be important (e.g. Kochanek 1991). The sharp increases in p_q seen in Fig. 9 (c) and (d) occur when $|u_g - u_c| \gtrsim 3$, and the smaller galaxies have core radii comparable to both their effective radius and to the scale over which the dispersion is measured. The massive increase in p_q is probably unrealistic, but a weaker form of the effect will occur.

The greatest assumption in these calculations is involved with the choice of R_f , the scale over which the line-

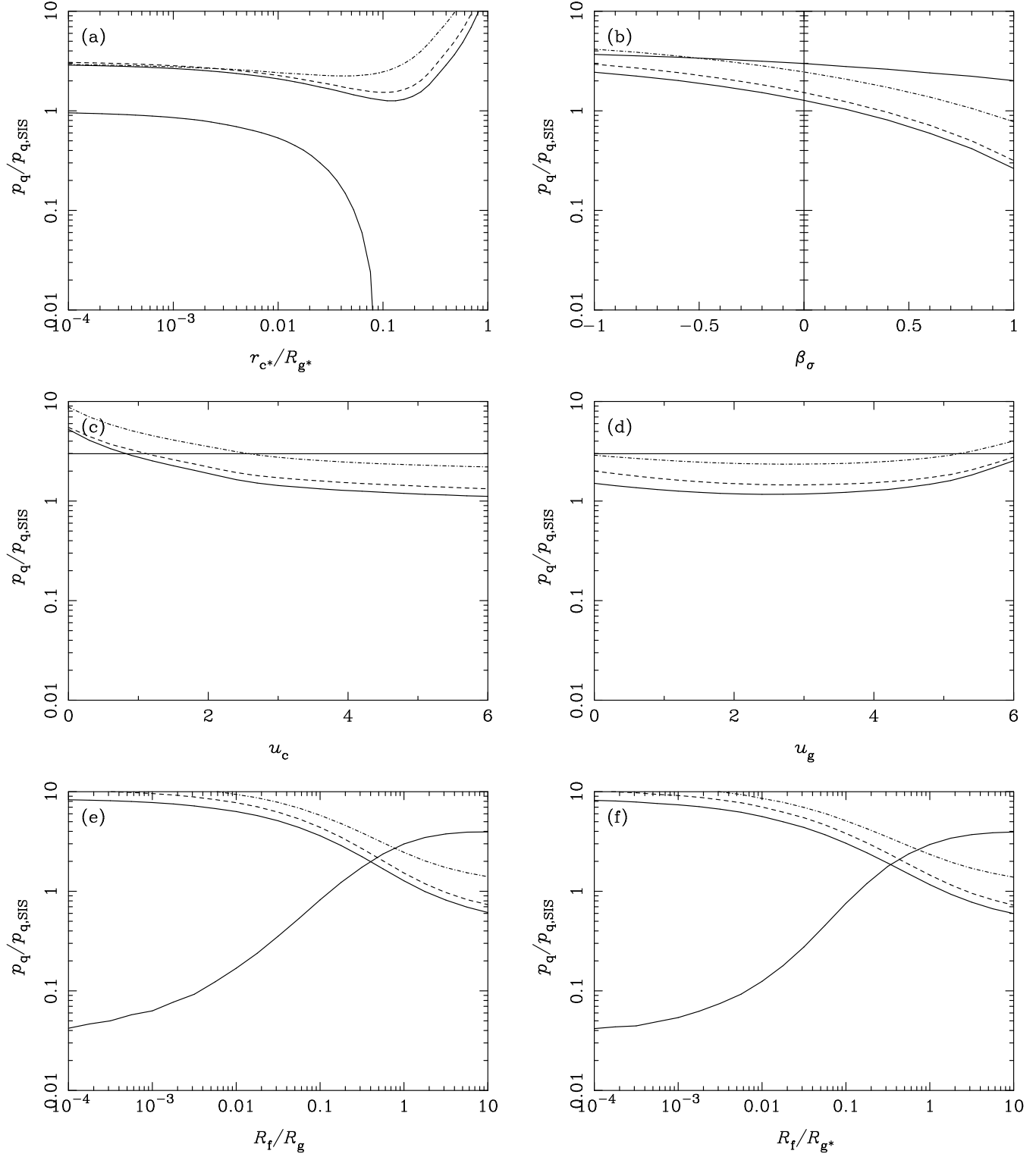


Figure 9. The probability that a $m_q = 19$, $z_q = 2$ quasar is lensed with $\Delta\theta \geq 1$ arcsec. It is scaled by the ‘standard’ lensing probability of a population of singular lenses with $\sigma_\infty = \sigma_{||}$. Three cosmological models are shown in each panel: $\Omega_{m0} = 1$ and $\Omega_{\Lambda 0} = 0$ (solid lines); $\Omega_{m0} = 0$ and $\Omega_{\Lambda 0} = 0$ (dashed lines); and $\Omega_{m0} = 0$ and $\Omega_{\Lambda 0} = 1$ (dot-dashed lines). The lower line in (a) is for $\sigma_\infty = \sigma_{||}$; the two sets of lines in panels (b), (c), (d), (e) and (f) represent $r_{c*} = 0$ (single line as there is no cosmological dependence) and $r_{c*} = 0.1R_{g*}$ (three distinct lines). The different panels show the dependence of p_q on: scale core radius, r_{c*} , in (a); velocity anisotropy, β_σ , in (b); core radius scaling exponent, u_c , in (c); effective radius scaling, u_g , in (d); and the aperture size, R_f , in (e) and (f). In (e) $R_f = R_g$, scaling with galaxy size; in (f) $R_f = R_{g*}$ and is constant. The default values used are: $\beta_\sigma = 0$; $u_c = 4$; $u_g = 4$; and $R_f = R_g$.

of-sight velocity dispersion is measured. Fig. 9 (e) and (f) show $p_q/p_{q,\text{SIS}}$ as a function of the typical scale of R_f ; in the former panel it scales with the effective radius of the galaxies, whereas in the latter it does not vary with the properties of the galaxy in question. If ellipticals are singular, a given observed dispersion results in a higher optical depth if $R_f \gtrsim R_g$, as the orbital speeds are much lower in the outer regions. Conversely, if ellipticals have significant core radii, the optical depth is highest for small apertures, in which case the measured dispersion is only a fraction of the dynamical normalisation. These arguments are true irrespective of how R_f scales with R_g , as can be seen from the similarity of panels (e) and (f) in Fig. 9.

3.3.1 Cosmological implications

The above formulation for p_q was extended to arbitrary cosmologies, the relevant distance and volume element formulae for which are given in e.g. Carroll et al. (1992). Fig. 10 shows the interdependence of p_q on the cosmological model and r_{c*} , both with and without the self-consistent dynamical normalisation. In the models with $\Omega_{\Lambda_0} = 0$ shown in (a), the core radius is considerably more important than the value of Ω_{m_0} , as expected. Further, the difference between the normalised and unnormalised models is greater than that between any $\Omega_{\Lambda_0} = 0$ cosmological model. The spatially-flat models shown in (b) have a much stronger cosmological dependence, but even then the core radius becomes more important as it approaches the effective radius of the lens galaxies. For more realistic values of r_{c*} , a slightly larger cosmological constant is permitted than if $r_{c*} = 0$, but not relative to the $\sigma_\infty = \sigma_{||}$ models. For instance, if a given dataset implied an upper limit of $\Omega_{\Lambda_0} \simeq 0.7$ for unnormalised singular lenses, the limit becomes lower ($\Omega_{\Lambda_0} \simeq 0.5$) with $\sigma_\infty \simeq 1.2\sigma_{||}$ singular galaxies. Even if $r_{c*} = 0.1R_g$, the upper limit on the cosmological constant would still be ~ 0.6 . The application of self-consistent dynamics shows that the standard models with $\sigma_\infty = \sigma_{||}$ and no core radius provide the weakest (i.e. very conservative) upper limits on Ω_{Λ_0} .

4 CONCLUSIONS

If the mass distribution of elliptical galaxies is essentially isothermal, one of the biggest uncertainties in their effect as gravitational lenses is their dynamical normalisation, σ_∞ . The mass scale depends on their internal dynamics (given by $\sigma_{||}$ and β_σ), the luminosity profile and the aperture used to calibrate the Faber-Jackson (1976) relation. A range of non-rotating, spherical galaxy models reveals that $\sigma_\infty \simeq 1.1\sigma_{||}$ for singular models, but that $1 \lesssim \sigma_\infty/\sigma_{||} \lesssim 2$ if ellipticals have significant core radii.

The dynamical normalisation can have a strong effect on both the lensing optical depth and the more correct lensing probability. In the case of the singular lens model, both are increased (by up to a factor of 2) by the application of the correct normalisation, irrespective of the cosmological model. The effect of the normalisation is even greater with the presence of a core radius. Both the optical depth and lensing probability increase with very large core radii, purely due to these self-consistency requirements. For a given observed Faber-Jackson (1976) relation, the optical depth can

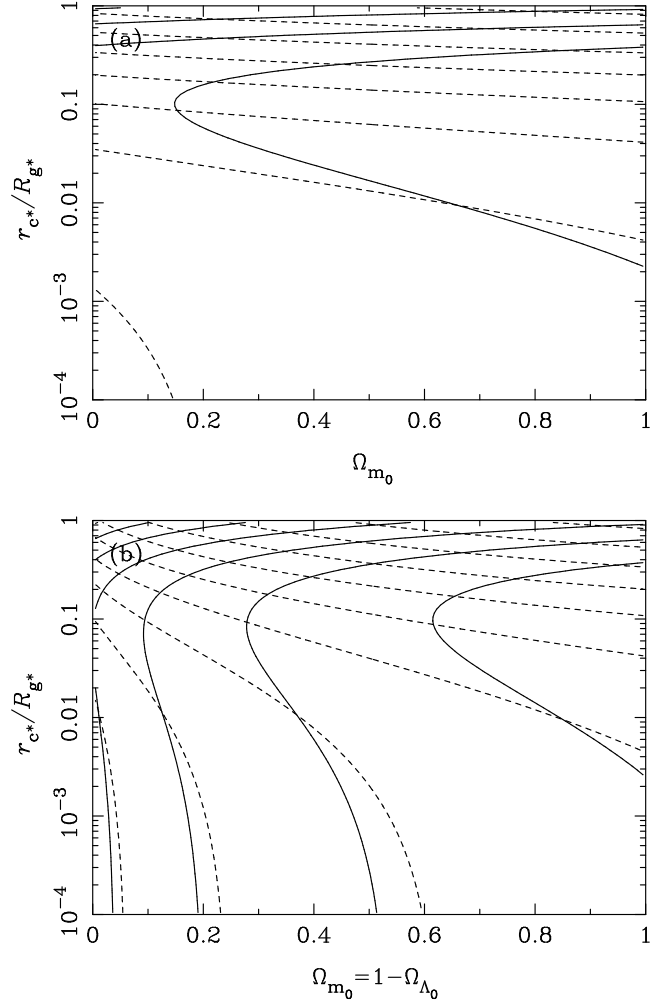


Figure 10. Contour plots showing the probability that a $m_q = 19$, $z_q = 2$ quasar is lensed with $\Delta\theta \geq 1$ arcsec, as a function of Ω_{m_0} and the canonical core radius, r_{c*} . In (a) there is no cosmological constant (i.e. $\Omega_{\Lambda_0} = 0$); in (b) the universe is spatially flat (i.e. $\Omega_{m_0} + \Omega_{\Lambda_0} = 1$). The contours are spaced logarithmically – three per decade. In (a) those for the unnormalised lens model (dashed lines) range from $p_q = 2 \times 10^{-6}$ to $p_q = 5 \times 10^{-4}$; those for the correctly-normalised model (solid lines) range from $p_q = 5 \times 10^{-4}$ to $p_q = 5 \times 10^{-3}$. In (b) those for the unnormalised lens model (dashed lines) range from $p_q = 2 \times 10^{-6}$ to $p_q = 2 \times 10^{-3}$; those for the correctly-normalised model (solid lines) range from $p_q = 5 \times 10^{-4}$ to $p_q = 5 \times 10^{-2}$.

vary by a factor of several with both the size of the dispersion aperture and the velocity anisotropy.

If lensing statistics are treated primarily as a cosmological probe, the above uncertainties place limits on the accuracy of any cosmological inferences. However, because the correct normalisation almost certainly increases the calculated lensing probability in a given cosmological model, it strengthens arguments against a high cosmological constant. The weakest limits on Ω_{Λ_0} obtained with the correct normalisation and an arbitrarily large core radius are comparable to the limits obtained for the standard singular models with $\sigma_\infty \simeq \sigma_{||}$. The dynamical conversions must be determined more precisely, theoretically and especially observationally, to make full use of gravitational lensing statistics.

ACKNOWLEDGMENTS

Many thanks to John Magorrian and Jon Willis for stimulating discussions. DJM was supported by an Australian Postgraduate Award.

REFERENCES

- Bahcall N. A., Fan X., Cen R. Y., 1997, *ApJ*, 485, L53
 Binney J. J., Tremaine S., 1987, *Galactic Dynamics*. Princeton University Press, Princeton
 Blandford R. D., Kochanek C. S., 1987, *ApJ*, 321, 658
 Boyle B. J., Croom S. M., Smith R. J., Shanks T., Miller L., Loaring N. S., 1999a, *Phil. Trans. of the Royal Soc. A*, 357, 185
 Boyle B. J., Croom S. M., Smith R. J., Shanks T., Miller L., Loaring N. S., 1999b, in Morganti R., Couch W. J., eds, *Looking Deep in the Southern Sky*. Springer-Verlag, Berlin, p. 16
 Boyle B. J., Shanks T., Peterson B. A., 1988, *MNRAS*, 235, 935
 Carroll S. M., Press W. H., Turner E. L., 1992, *ARA&A*, 30, 499
 Colless M. M., 1999, in Morganti R., Couch W. J., eds, *Looking Deep in the Southern Sky*. Springer-Verlag, Berlin, p. 9
 de Vaucouleurs G., 1948, *Annalen d'Astrophysics*, 11, 247
 de Vaucouleurs G., Olson D. W., 1982, *ApJ*, 256, 346
 Dressler A., Lynden-Bell D., Burnstein D., Davies R. L., Faber S. M., Terlevich R. J., Wegner G., 1987, *ApJ*, 502, 550
 Dyer C. C., Roeder R., 1972, *ApJ*, 174, L115
 Dyer C. C., Roeder R., 1973, *ApJ*, 180, L31
 Efstathiou G., Bridle S. L., Lasenby A. N., Hobson M. P., Ellis R. S., 1999, *MNRAS*, 303, L47
 Efstathiou G., Ellis R. S., Peterson B. A., 1988, *MNRAS*, 232, 431
 Faber S. M., Jackson R. E., 1976, *ApJ*, 204, 668
 Falco E. E., Kochanek C. S., Muñoz J. A., 1998, *ApJ*, 494, 47
 Falco E. E., et al., 1999, *ApJ*, 523, 617
 Folkes S. R., et al., 1999, *MNRAS*, 308, 459
 Fukugita M., Turner E. L., 1991, *MNRAS*, 253, 99
 Fukugita M., Futumase T., Kasai M., 1990, *MNRAS*, 246, 24
 Gott J. R., 1977, *ARA&A*, 15, 235
 Guth A. H., 1981, *Phys. Rev. D*, 23, 347
 Hernquist L., 1990, *ApJ*, 356, 359
 Hinshaw G., Krauss L. M., 1987, *ApJ*, 320, 468
 Kassiola A., Kovner I., 1993, *ApJ*, 417, 450
 Kayser R., Helbig P., Schramm T., 1997, *A&A*, 318, 680
 Keeton C., Kochanek C. S., 1996, in Kochanek C. S., Hewitt J. N., eds, *Proc. IAU Symp. No. 173. Astrophysical Applications of Gravitational Lensing*. Kluwer, Dordrecht, p. 419
 Keeton C., Kochanek C. S., Falco E. E., 1998, *ApJ*, 509, 561
 Kochanek C. S., 1991, *ApJ*, 379, 517
 Kochanek C. S., 1992, *ApJ*, 384, 1
 Kochanek C. S., 1993, *ApJ*, 419, 12
 Kochanek C. S., 1994, *ApJ*, 436, 56
 Kochanek C. S., 1995, *ApJ*, 453, 545
 Kochanek C. S., 1996a, in Kochanek C. S., Hewitt J. N., eds, *Proc. IAU Symp. No. 173. Astrophysical Applications of Gravitational Lensing*. Kluwer, Dordrecht, p. 7
 Kochanek C. S., 1996b, *ApJ*, 466, 638
 Kochanek C. S., Blandford R. D., 1987, *ApJ*, 321, 676
 Kochanek C. S., Falco E. E., Impey C. D., Lehár J., McLeod B. A., Rix H.-W., 1999, in Holt S., Smith E., eds, *Am. Inst. Phys. Conf. Proc. 470, After the Dark Ages: When Galaxies Were Young (The Universe at $2 < z < 5$)*. Am. Inst. Phys., Baltimore, p. 163
 Kochanek C. S., et al., 2000, *ApJ*, in press
 Kolb E. W., Turner M. S., 1989, *The Early Universe*. Addison-Wesley Publishing Company, Redwood City
 Kormendy J., Djorgovski G., 1989, *ARA&A*, 27, 235
 Kormendy J., Richstone D., 1995, *ARA&A*, 33, 581
 Kormendy J., et al., 1996, *ApJ*, 473, L91
 Kormendy J., et al., 1997, *ApJ*, 482, L139
 Krauss L. M., White M., 1992, *ApJ*, 394, 385
 Lauer T. R., et al., 1995, *AJ*, 110, 2622
 Lineweaver C. H., 1998, *ApJ*, 505, L69
 Loveday J., Pier J., 1998, in Colombi S., Mellier Y., Raban B., eds, *Wide Field Surveys in Cosmology*. Edition Frontiers, Paris, p. 317
 Malhotra S., Rhoads J. E., Turner E. L., 1997, *MNRAS*, 288, 138
 Mao S., 1991, *ApJ*, 380, 9
 Mao S., Kochanek C. S., 1994, *MNRAS*, 268, 569
 Maoz D., Rix H.-W., 1993, *ApJ*, 416, 425
 Mortlock D. J., 1999, PhD Thesis, University of Melbourne
 Mortlock D. J., Webster R. L., 2000a, *MNRAS*, in press
 Mortlock D. J., Webster R. L., 2000b, *MNRAS*, in press
 Navarro J. F., Frenk C. S., White S. D. M., 1996, *ApJ*, 462, 563
 Navarro J. F., Frenk C. S., White S. D. M., 1997, *ApJ*, 490, 493
 Perlmutter S., et al., 1999, *ApJ*, 517, 565
 Press W. H., Gunn J. E., 1973, *ApJ*, 185, 397
 Rix H.-W., Maoz D., Turner E. L., Fukugita M., 1994, *ApJ*, 435, 49
 Schechter P., 1976, *ApJ*, 203, 297
 Schmidt B. P., et al., 1998, *ApJ*, 507, 46
 Schneider P., Ehlers J., Falco E. E., 1992, *Gravitational Lenses*. Springer-Verlag, Berlin
 Subramanian K., Cowling S. A., 1986, *MNRAS*, 219, 333
 Szalay A. S., 1998, in Müller V., Gottlöber S., Mücke J. P., Wambsganss J., eds, *Large Scale Structure: Tracks and Traces*. World Scientific, Singapore, p. 97
 Turner E. L., 1980, *ApJ*, 242, L135
 Turner E. L., 1990, *ApJ*, 365, L43
 Turner E. L., Ostriker J. P., Gott J. R., 1984, *ApJ*, 284, 1
 van der Marel R. P., 1991, *MNRAS*, 253, 710
 Wallington S., Narayan R., 1993, *ApJ*, 403, 517
 Young P. J., 1976, *ApJ*, 81, 807

This paper has been produced using the Royal Astronomical Society/Blackwell Science L^AT_EX style file.